EXAFS in liquids and disordered systems: a personal review

A. Di Cicco*
Physics Division, School of Science and Technology, Università di Camerino, Via Madonna delle Carceri 62032, Camerino (MC), Italy
**recipient of the outstanding achievement IXAS award (Stern Prize) in 2015*
(Dated: October 16, 2016)

Some of the most interesting achievements in the application of XAS to disordered systems are reviewed from a personal perspective. In this work, the continued efforts in studying liquids and disordered systems by the x-ray absorption spectroscopy (XAS) in the last decades are reviewed by examples of applications to selected substances. Experimental and data-analysis methods, proven to be successful in dealing with highly disordered systems, are briefly summarized highlighting the potential of the XAS technique. Experiments and results obtained under high-pressure and/or high temperature conditions are also mentioned in connection with present experimental and computational capabilities.
Published in: *XAS Research Review, webmag. of the Intern. XAFS soc.,* **15***, February 2016.*

I. INTRODUCTION

In this contribution I try to outline and place in a possibly general context some of the achievements related to the "outstanding achievement award" (Stern Prize) of the International XAS society, obtained in 2015 for pioneering work in the application to disordered systems.

The x-ray absorption spectroscopy (XAS) and in particular the so-called EXAFS (Extended X-ray Absorption Fine Structure) technique is now recognized as an extremely powerful and accurate method for the determination of the local structure in different thermodynamic conditions spanning the phase diagram of a variety of substances, including appearance of metastable and transient states.

Important aspects of the evolution of XAS in the last decades have been both the development of advanced data-analysis approaches and of suitable methods for performance of accurate experiments under non-standard conditions. In particular, accurate and reliable multiple-scattering calculations were developed since 1975 by various authors. Advanced EXAFS data-analysis methods based on multiple-scattering simulations were gradually developed in U.K. at Daresbury (EXCURVE[2] with later fitting implementations, EXCURV98), in Italy at Frascati (GNXAS[3]), and in U.S.A. at Seattle (FEFF, using fitting routines like FEFFIT[4]). The importance of performing EXAFS experiments in glasses and liquids was soon understood, due to its unique sensitivity to the short-range structure. However, structural refinements of disordered systems required suitable developments of data-analysis techniques (see Sec. II), among which GNXAS played a major role. Further developments included extensive use of computer simulations (namely Monte-Carlo, Molecular Dynamics, and Reverse Monte-Carlo) improving our insight on the local structure in disordered substances.

In parallel, several experimental advances allowed us performance of reliable and accurate XAS experiments of disordered systems also under extreme conditions, for example at high temperature and/or high pressure. Examples of XAS experiments and results on disordered substances are briefly reviewed in Sec. III.

II. XAS THEORY AND DATA-ANALYSIS FOR DISORDERED SUBSTANCES

The application to disordered systems, and especially to liquids, required particular efforts in treating the configurational averages of the MS contributions. The theoretical framework embedded within the GNXAS (n-body expansion) method[3,5–8] was found to be ideally suited for a correct application of the configurational average through the n-body distribution functions (pair, triplet and so on). The fundamental equation relating the n-body (n=2,3, ...) distribution functions $g_n(r)$ and the XAS structural signal $\chi(k)$, is the following:

$$\chi_\alpha(k) = \sum_\beta \int_0^\infty 4\pi\rho_\beta r^2 g_2^{\alpha\beta}(r)\ \gamma_\beta^{(2)}(k,r)\ dr + \sum_{\beta\beta'} \int dr_1 dr_2 d\theta\ 8\pi^2 r_1^2 r_2^2 \sin(\theta)\rho_\beta\rho_{\beta'} \times g_3^{\alpha\beta\beta'}(r_1,r_2,\theta)\ \gamma_{\beta\beta'}^{(3)}(r_1,r_2,\theta,k) + \quad \cdots \quad (1)$$

from which $\chi_\alpha(k)$ can be calculated by integration. The XAS signal $\chi_\alpha(k)$, related to a selected chemical species α (measured tuning the photon energy to a selected core level excitation), is a function of the photoelectron wave-vector k usually measurable in a range extended to 10-30 Å^{-1}. α, β, and β' are chemical species of the (multi-component) system under consideration, while ρ_β ($\rho_{\beta'}$) are the corresponding partial densities. The irreducible two-body (pair) $\gamma_\beta^{(2)}(k,r)$ signals are oscillating function in k (leading phase is $2kr$) with an amplitude decreasing exponentially with r, and can be calculated directly with the `gnxas` program. Three-body $\gamma_{\beta\beta'}^{(3)}(k,r_1,r_2,\theta)$ signals depend on triangular coordinates (being r_1, r_2 usually the shortest interatomic distances and θ the angle among them). They are also oscillating functions rapidly decaying with the distances, with the

exception of special cases (for example collinear configurations). Expression (1) truncated to the pair distribution (n =2) is usually a reasonable approximation for highly disordered systems in the EXAFS regime. Moreover, $\gamma^{(2)}_{\beta}(k,r)$ can be usually approximated by its single scattering expression at large k values.

A simple peak-fitting technique, modelling the pair distribution function $g(r)$ (and higher-order ones) as a sum of distinct Gaussian or slightly asymmetric peaks, can be used for most XAS applications in solid systems and is computationally faster. This approach is adopted by GNXAS and implemented in the program `fitheo` which provides the structural refinement in terms of parameters defining the pair distribution[7,8]. The program `fitheo` provides best-fit values for the structural parameters and error bars (including correlation maps) considering the raw experimental data with no Fourier filtering. Using raw EXAFS data has been found to be extremely useful to avoid systematic errors in the structural refinement, due to incorrect background modelling, and to assess realistic uncertainty values to the structural parameters as a consequence of the noise level in the measurements.

For liquids, however, being XAS substantially blind to medium and long-range ordering, it is necessary to introduce suitable constraints for medium and long-range structure.[7–10] These constraints can be introduced for mono-atomic[11] and binary liquids[12] in the framework of the peak-fitting technique, and proper subroutines were included in the `fitheo` program (GNXAS)[7,8] accounting for the correct long-range behavior of the pair distribution functions. It is important to remark that refinements of the local structure of liquids neglecting those constraints can lead to erroneous results. In liquid Pb, for example, the first-neighbor coordination number was found to decrease to about 50 % the crystalline value (12) using a simple non-constrained peak-fitting approach[13]. Lead is instead known to be, since the first neutron and x-ray scattering experiments, a close-packing liquid with first-neighbor coordination approaching 12. The reason for such a discrepancy is related to the strong correlation between standard XAS peak-fitting parameters (coordination N and bond variance σ^2) but this example epitomizes the importance of a correct XAS data-analysis and treatment of disorder. As shown in many successive papers, the pair distribution obtained by XAS using modern data-analysis methods like GNXAS was shown to be consistent and in excellent agreement with previous estimates (see the next Sec. III and simple examples like Ge,[9] and Ga[14]). In the case of liquid Pb (see ref. 15), XAS was found to be consistent with previous diffraction data and was also used to discriminate between various models in light of the XAS sensitivity to the short-range structure. As an example of the importance of application of those techniques to liquid systems I also recall the important improvement in our understanding of the short-range structure in molten salts, missing in previous challenging time-consuming neutron diffraction data obtained with the isotope-substitution technique (see[16] and refs. therein).

Reverse Monte Carlo (RMC) refinements[17,18] were also used to build realistic models of the tridimensional structure of disordered systems, overcoming the limitations of the model-dependent peak-fitting technique. Within this approach, the average structure resulting from a simulation including thousands of atoms in a box is refined (moving the atomic positions) until being compatible with a set of experimental data. The `rmcxas` program of the RMC-GNXAS package is fully interfaced with GNXAS[8] and performs standard RMC structural refinements of both molecular and condensed structures. The χ^2 function at each RMC step is given by:

$$\chi^2 = \sum_{i=1}^{N_{XAS}} \left[\chi^E(k_i) - \chi^C(k_i)\right]^2 / \sigma_i^2 + \sum_{j=1}^{N_g} \left[g_2^E(r_j) - g_2^C(r_j)\right]^2 / \sigma_j^2 \qquad (2)$$

where in the first term of the r.h.s. χ^C is calculated starting from the actual atomic coordinates using Eq. 1 and the $\gamma^{(2)}$ signals given by GNXAS, χ^E is the raw XAS signal determined by a preliminary data-analysis (performed using the `fitheo` program, GNXAS suite) and σ_i^2 the noise function obtained from the experiment (possibly evaluated by `fitheo`). In the second term (omitted in molecular cases) g_2^C is the pair distribution associated with the atomic coordinates of the RMC box, g_2^E is a model pair distribution obtained by neutron/x-ray diffraction or computer simulations, and σ_j^2 is the variance associated with the pair distribution.

The application of RMC to EXAFS data of liquids[17,19–21] has shown that reliable model-independent pair distribution functions can be extracted by considering both EXAFS and diffraction $g(r)$ data, for short and medium-long range correlations respectively. In Fig. 1 I report the results of the RMC refinement of the EXAFS spectrum of liquid Cu[17,19] as an example. The trend of the χ^2 residual function (defined in Eq. 2) shows that convergence to the expected vale can be reached within a reasonable number of RMC moves. A crucial point for faster convergence is the preparation of an initial structure compatible with the pair distribution function g_2^E chosen for the minimization in Eq. 2. The XAS $k\chi(k)$ structural signal of liquid Cu (l-Cu) is compared with the two-body component of the RMC simulation $k\gamma^{(2)}(k)$ in Fig. 1 (upper inset). The RMC curve reproduces the shape of the ND[22] and XRD[23] $g_2(r)$ above about 4 Å while the first-neighbor peak is slightly narrower and shifted to shorter distances, as a consequence of the unique sensitivity of the XAS signal. On the other hand, the high-frequency oscillation of the residual curve shows that the simple two-body $k\gamma^{(2)}$ contribution does not fully reproduce the experimental indicating that higher order terms have to be included in the simulation. The difference spectrum $k\left(\chi(k) - \gamma^{(2)}\right)$ (shown on an enhanced scale) is compared with a XAS three-body signal

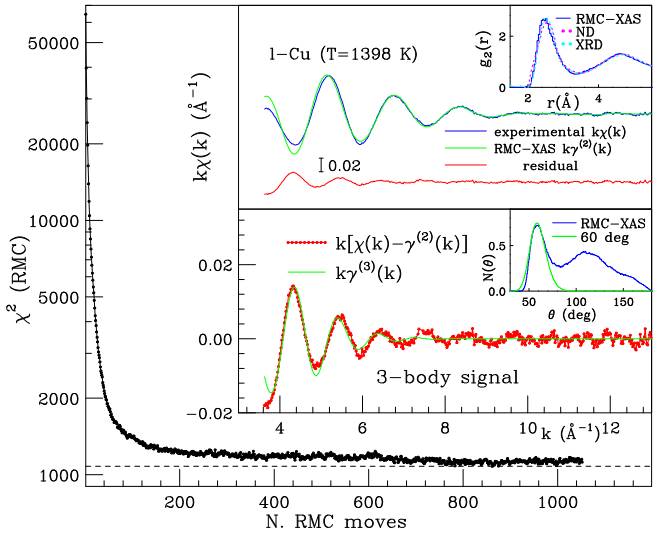

FIG. 1. Trend of the χ^2 residual function converging to a minimum during the RMC simulation in liquid Cu at 1398 K. The inset (upper panel) shows the Cu K-edge EXAFS experimental data (l-Cu) compared with the two-body component of the RMC multiple-scattering simulation. The residual lower curve shows that three-body terms have to be included to simulate the whole XAS spectrum. The small upper inset shows the pair correlation function $g_2(r)$ associated with the RMC simulation and previous determinations using neutron (ND) and x-ray (XRD) diffraction. The difference spectrum is in excellent agreement (lower panel) with the XAS three-body signal calculated using a Gaussian three-body distribution for equilateral triangles. The full bond-angle $N(\theta)$ distribution resulting from the RMC simulation is compared with that of the equilateral triangles in the small inset.

calculated using a Gaussian three-body distribution for equilateral triangles (lower inset of Fig. 1). In fact, the main component of the XAS three-body signal is associated with the peak of the bond-angle $N(\theta)$ distribution associated with nearly-equilateral triangular configurations, as shown in the small inset. Details of this study and its relevance for understanding the structure of liquid metals can be found in refs. 17, 19, and 20.

III. XAS OF LIQUIDS AND GLASSES AT HIGH TEMPERATURE/PRESSURE

Many successful XAS applications to liquids, as well as relevant experimental and data-analysis techniques, are described in the beautiful review written by A. Filipponi[10]. In particular, the XAS technique was applied to several liquid metals (elemental and alloys) all along the periodic table. First experiments of the early 90s were carried out at Frascati (PULS, ADONE storage ring) and LURE (DCI, Orsay) on emulsion of Ga[14,24] and Hg[25,26] droplets and on In, Sn,[27] Pb, and Bi films. Molecular liquids like liquid Br_2,[28] as well as some liquid solutions,[29] were also measured at that time. Those measurements were limited to temperatures reachable with readily available temperature devices (cryostats and furnaces for moderate high temperature around 700 K) but the success of these initial efforts, including production of the first samples of nearly-uniform thickness, leaded soon to the development of a new furnace for x-ray experiments[30,31]. Suitable XAS samples of liquid systems were mostly obtained by mixing the investigated substances in form of fine powders (or droplets) with low x-ray absorbing non-reacting materials (typically ultrapure boron nitride, carbon) in the typical form of compressed pellets. Dispersions of pure (liquid) substances were obtained either using starting ultrapure materials or by in-situ reduction processes at high temperature. For example, extremely good samples for Cu K-edge XAS of liquid copper were obtained by in-situ reduction of copper oxide (mixed with graphite or BN).

The possibility of achieving extremely high undercooling rates for elemental liquid systems was also recognized immediately, in polymorphic low-melting point metals like Ga and Hg. Emulsions of Ga droplets in epoxy resin were found to show exceptional undercooling down to 150 K, and a combination of techniques was used for this purpose (XAS, single-energy temperature scans, x-ray diffraction, electrical resistivity)[32,33]. In particular, x-ray single-energy temperature scans[34] were developed and shown to be effective to detect phase transitions and hysteresis loops in ordered and disordered systems. In Fig. 2 I report some x-ray single-energy temperature results obtained for dispersions of metal droplets (grains when crystalline) in very different hosting materials. Typically, the photon energy is chosen in the vicinity of the absorption edges, maximizing the contrast among the XAS signals associated with the different phases. In Fig. 2, the temperature scale has been normalized to the (very different) melting points (T_m= 303, 1358, 1728 K for Ga, Cu, Ni respectively) in order to compare directly the undercooling rates. As shown in Fig. 2, sharp transitions are observed at the melting points, while re-crystallization takes place usually more gradually, lowering the temperature. Undercooling limits and shape of the crystallization curve depend on various factors including distribution, dimension and shape of the metal particles, purity, and interaction with the hosting material. The remarkable undercooling record obtained for Ga (150 K) was obtained by mixing submicrometric Ga droplets with epoxy resin, and the lowering of melting point to about 254 K is due to the confinement of Ga grains[32] which prevent crystallization to the stable Ga-I (α) phase having a lower density than liquid Ga. Single-energy temperature scans of liquid Cu and Ni shown in Fig. 2 were collected using a high-temperature furnace[30,35,36] developed for combined XAS and XRD measurements. Cu and Ni show quite different undercooling rates in this example, but this is likely to be due mostly to the different materials used as a container (graphite and alumina), which may favor formation of crystal seeds, and to the different droplet

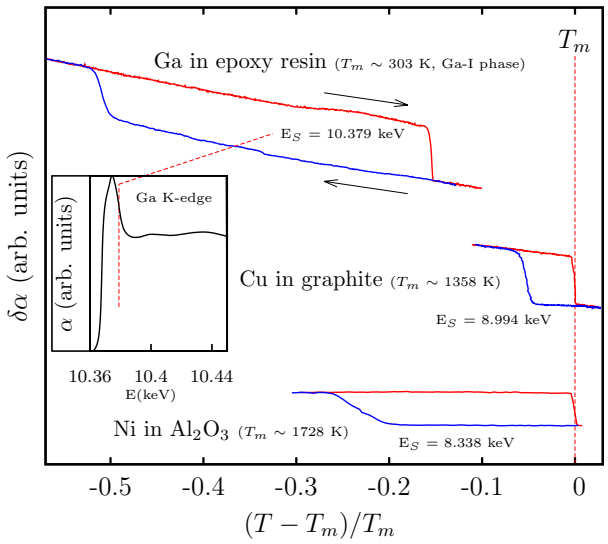

FIG. 2. Single-energy x-ray absorption temperature scans for different metals (see refs. 17, 21, and 33), reported on a temperature scale normalized to the melting point T_m of each metal (Ga, Cu, Ni, see figure). Photon energy for the scans were chosen to maximize the contrast between liquid and solid phases, in the vicinity of the K-edge of each metal (Ga case is reported in the inset). Large undercooling rates are observed in dispersion of (sub)micrometric metal droplets as shown by the hysteresis loops in the figure (heating are the red, upper, lines and cooling are the blue, lower, lines). Undercooling rates depend strongly on the metal, droplet dimensions and of the material used as a container (epoxy resin, graphite, alumina for Ga, Cu, and Ni respectively). The exceptional undercooling of Ga[32] is due to the peculiar ice-type behavior of this element and the shift of melting point is due to its confinement in epoxy resin.

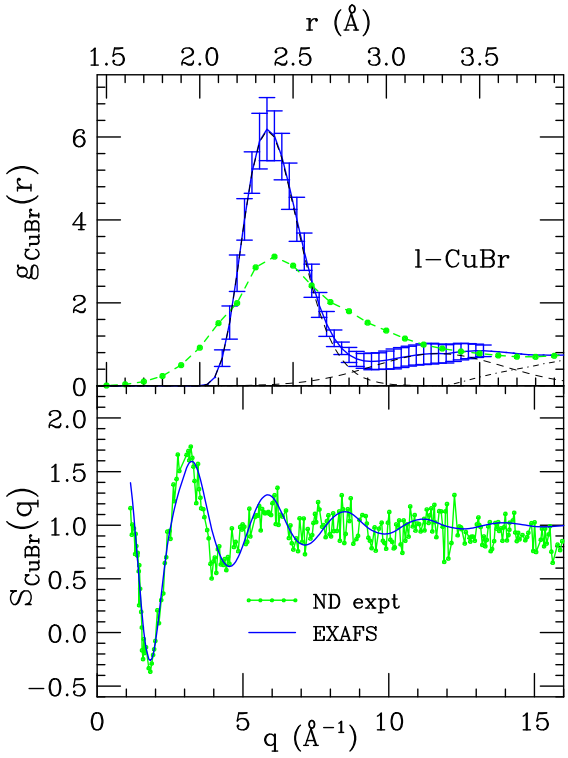

FIG. 3. Upper panel: comparison between $g_{CuBr}(r)$ determination by neutron diffraction (ND expt, green) and XAS double-edge refinement (EXAFS, blue)[16]. Dashed and dot-dashed curves are the short-range part (peak-fitting approach) and the tail of the distribution functions. The error bars indicate the estimated accuracy of the EXAFS refinements. Lower panel: comparison of the partial structure factor $S_{CuBr}(q)$ as derived by isotope-substitution neutron diffraction measurements (ND expt)[48], and the reconstructed $S(q)$ obtained by XAS refinement (EXAFS).

size distributions.

As discussed above, XAS provided important insight about the local structure in many "simple" liquid systems including liquid metals and alloys, liquid solutions (see for example the continued efforts of the P. D'Angelo group[29,37,38]), and molten salts. Binary molten salts are probably among the simplest liquid systems, and reliable modeling of the inter-atomic interactions and average structure are available by experiments and computer simulations (see for example 16, 39, and 40 and refs. therein). However, structure and properties of the so-called superionic binary systems like CuBr, AgI and AgBr are more difficult to understand and modeling, due to the elevated mobility of the metal ions also in the solid phases. These materials were investigated using XAS since the early times (see[41,42]) showing the potential of this technique. However, the mentioned advances in experiments and theory achieved in the 90s made possible a direct comparison of XAS, neutron diffraction and computer simulation results. In particular, multiple-edge XAS analysis was applied to CuBr[16,43] (and later to AgBr[44], AgI[45], and CuI[46], and also to mixtures[47] of them) and structural results were compared with diffraction data.

In Fig. 3, upper panel, the $g_{CuBr}(r)$ pair distribution functions in liquid CuBr at T=793 K obtained by double-edge EXAFS refinement[16,43] and by neutron diffraction[48] ND (isotope-substitution technique) are compared. The two short-range refinements are remarkably different, reflecting the different sensitivity of the two techniques. In fact, the EXAFS reconstructed structure factor $S(q)$ (using the much sharper $g_{CuBr}(r)$ probed by EXAFS) is clearly compatible with the original ND data. This remarkable result shows clearly that the unique short-range sensitivity of the XAS technique can be used to obtain reliable measurements of short-range ordering in liquids, complementing medium and long-range order information obtained by diffraction.

For the sake of completeness, I also mention XAS applications to high-pressure liquids, in the limited space offered by this short review. In fact, XAS can be quite easily applied to materials measured in static condi-

tions under pressures in the 10 GPa range with large-volume cells and in the MBar range (100 GPa) using diamond anvil cells (see for example 49 and refs. therein). Using XAS, metastable states including deep undercooled liquids under static pressure can be measured using well-established techniques (see for example 19 and 50) opening scientific explorations of high-pressure metastable states previously impossible. Moreover, liquids and highly-excited systems can be also measured under transient conditions with various ultrafast techniques[51], using time-resolved spectroscopies at synchrotron beamlines (see for example refs. 52 and 53) or at free-electron laser facilities (see for example refs. 54–56).

Glasses and amorphous systems have been investigated since the advent of XAS spectroscopy and a complete review is certainly beyond the scope of this contribution. Anyway, in the last decade several efforts were spent for carrying out XAS experiments on glasses under high pressure conditions. This has been favored by important improvements at the beamlines allowing for performance of reliable and accurate experiments under extreme conditions (see for example 49 and refs. therein). In particular, significant efforts were devoted to the study of transformations of the local structure in glasses under pressure, hunting peculiar transitions between low-density (LDA) and high-density (HDA) amorphous structures. Early examples include the fourfold to sixfold coordination change in glassy GeO_2 probed by XAS[57]. Recently, evidence of glass polymorphism was obtained in amorphous Ge[58] and several other systems. A clear LDA-HDA (semiconductor to metal) sharp transition was observed at about 8 GPa by combining XAS, Raman scattering, and XRD techniques,[59–61] later also confirmed by ab-initio calculations[62].

XAS has been also recently applied for understanding the evolution of short-range ordering in compressed archetypal chalcogenide glasses like $GeSe_2$ and As_2Se_3. The question about the effect of compression on local ordering around both atomic species (Ge, Se in $GeSe_2$) was answered by using a combination of double-edge XAS and XRD experiments[63] and I report here the results obtained by Properzi et al. as an example of gradual LDA to HDA transitions.

The quality of the experiments can be appreciated looking at the comparison between the Ge K-edge XAS structural signals ($\chi(k)$) for crystalline (c-$GeSe_2$) and amorphous (a-$GeSe_2$) materials shown in Fig. 4 (left panel) at ambient pressure. Se K-edge data are of very similar quality[63]. Structural double-edge refinement[27,44] of XAS spectra was carried out by using GNXAS providing direct information on the (partial) pair distribution functions (Ge-Se, Se-Se, Ge-Ge). The first neighbor distribution related to the Ge-Se covalent bonding is associated with the dominant Ge-Se (Se-Ge) two-body signal reproducing most of the EXAFS spectral features both for c-$GeSe_2$ and a-$GeSe_2$. For c-$GeSe_2$ the first-neighbor distribution is found to be in agreement with the known crystal structure (see Ref. 64 and refs.

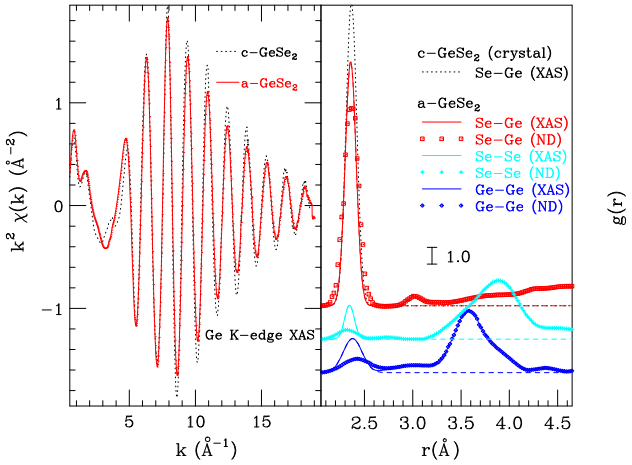

FIG. 4. The Ge K-edge XAS signals of crystalline (c-$GeSe_2$, dots) and amorphous (a-$GeSe_2$) are compared in the left panel. Differences in the low k region and in the XAS amplitude are related to the different short-range ordering of the two systems. The Se-Ge, Ge-Ge, and Se-Se partial distribution functions in a-$GeSe_2$ as measured by multiple-edge XAS and neutron-diffraction (ND) are shown and compared with the Ge-Se distribution in c-$GeSe_2$ (right hand-side panel).

therein), with fixed coordination numbers ($N_{GeSe} = 4$, $N_{SeGe} = 2$). The XAS structural refinement of the short-range structure of a-$GeSe_2$ takes into account previous results obtained by neutron-diffraction[65]. In particular, partial radial distribution functions obtained by neutron diffraction indicated occurrence of chemical disorder in a-$GeSe_2$, leading to the formation of first-neighbor Ge-Ge and Se-Se bonds[65,66]. Chemical disorder was included in XAS refinements of a-$GeSe_2$ allowing for the presence of first-neighbor Ge-Ge and Se-Se bonds with the constraint of keeping fixed the total coordination number ($N_{GeSe} = 4$, $N_{SeGe} = 2$) and stoichiometry. The improvement of the fit obtained by introducing a moderate chemical disorder was found to be statistically meaningful. Here, the possibility of detection of chemical disorder is mainly due to the strong constraints imposed by the double-edge refinement and by the extended k-space fitting on raw data[27]. Average Ge-Se first-neighbor distance and bond variance were found in substantial agreement with previous EXAFS analysis conducted on Ge-Se glasses[67]. In the right-hand side panel of Fig. 4 we report the partial pair distributions resulting by present XAS data-analysis, showing that present refinement is in substantial agreement with previous neutron-diffraction (ND) results.[65] Due to the intrinsic short-range nature of the XAS probe, only first-neighbor $g(r)$ peaks (below 2.5 Å in Fig. 4) are accurately measured, but present XAS structural refinement anyway confirms previous ND results about the presence of chemical disorder in $GeSe_2$, indicating that the bond distributions of like-like and like-unlike first-neighbors are well-defined peaks associated with nearly-covalent bonding[63].

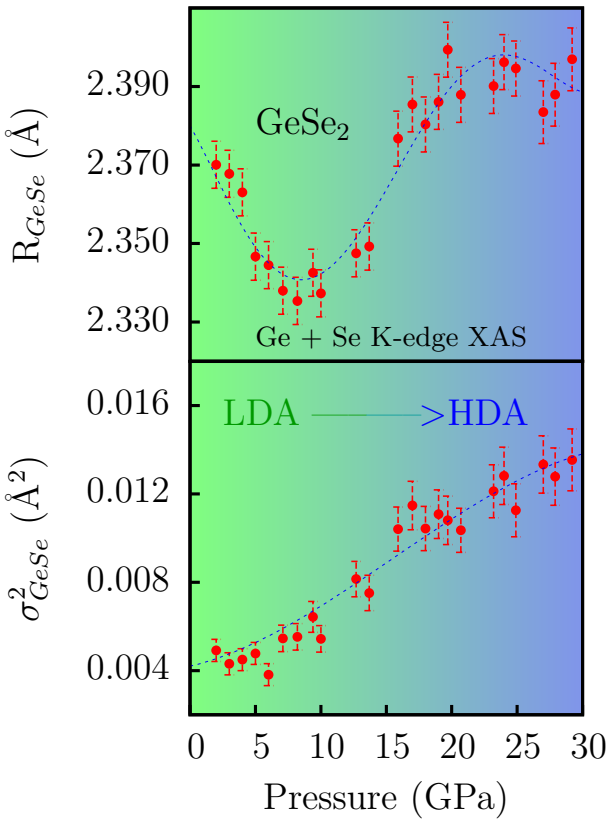

FIG. 5. Double-edge XAS best-fit results for the first-neighbor Ge-Se distance (R_{GeSe}) and bond variance (σ^2_{GeSe}) as a function of pressure for a-$GeSe_2$. The material remains amorphous at all pressures and a transition from a low-density (LDA) to a high-density amorphous (HDA) takes place upon pressurization, as monitored by the change of slope in the bond distance between 10 and 15 GPa. The color gradient is a guide for the eye.

The evolution of the local structure of a-$GeSe_2$ with pressure was studied combining dispersive XAS and XRD measurements up to 32.5 GPa (ODE beamline at Soleil). The sample was found to remain amorphous up to the highest pressures attained, and a reversible red-shift of the Ge K-edge energy, of about 1.5 eV, was observed above 10 GPa up to about 15 GPa[63]. This shift is interpreted as the signature of a metallization process associated with the appearance of a delocalized electron states prevalently around the Ge sites. Interestingly, a similar shift was not observed at the Se K-edge.

Several Ge and Se K-edge EXAFS spectra were collected at each pressure point, and results combined to give several sets of double-edge best-fit parameters for which average values are presented in Fig. 5. As shown in Fig. 5 (upper panel), the first-neighbor Ge-Se average distance $R_{GeSe}$is first decreasing and then increasing for pressures above 10 GPa. In the lower part of Fig. 5, I report also the Ge-Se bond variance σ^2_{GeSe} obtained by double-edge XAS refinement. The bond variance, associated with structural disorder, is found to increase in the entire pressure range. This is an expected behavior for an amorphous material when further atoms has to be accommodated at short distances by compression, breaking the more ordered and symmetric fourfold coordination (Ge sites). The increase in the average first-shell distance is related also by a corresponding first-neighbor coordination increase. A gradual increase in the first-neighbor coordination number is predicted by MD simulations[68], and the mean Ge-Se coordination is estimated around 4.5 at 9.3 GPa by XRD[69]. Molecular Dynamics (MD) simulations for a-$GeSe_2$ has shown the average germanium coordination reaching ∼5.5 at about 30 GPa[68]. Due to the known correlation among bond variance and coordination number parameters, EXAFS fitting procedures included a variation of the average Ge-Se coordination number following the pressure trend obtained by MD calculations[68].

The fact that the bond variance (mean square relative displacement) is found still to increase at limiting pressures is seen as an evidence that the conversion to the octahedral configuration (HDA) is not yet completed. This result is in agreement with previous MD simulations[68], predicting a full conversion to octahedral coordination only at pressures around 50 GPa. Generally speaking, the compaction mechanism seems to be analogous to what happens in similar systems such as GeO_2 and GeS_2[57,70].

In particular, present EXAFS data allowed us distinguish two compression stages: i) decrease of the first-neighbor distances up to about 10 GPa, in the same pressure region of the breakdown of the intermediate-range order previously observed by XRD[69]; ii) increase of the first-shell average distance and bond fluctuations, and of the coordination number. This second stage is related to a reversible non-isostructural transition involving a gradual conversion from tetra- (LDA) to octa-hedral (HDA) geometry which is not found to be fully completed at pressures up to 30 GPa.

IV. ACKNOWLEDGMENTS

I am indebted to A. Filipponi, for his generosity in sharing with me his intuitions, deep understanding of physics, and enthusiasm for experiments and theory. I am also indebted to C. R. Natoli (Rino) who taught me some secrets of multiple-scattering calculations and his “vision” for the connection between theory and experiments.

[1] XAS Research Review, webmagazine of the International XAFS society, vol. 15, February issue (2016).

[2] S. J. Gurman, N. Binsted, and I. Ross, J. Phys. C **19**, 1845 (1986).

[3] A. Filipponi, A. Di Cicco, T. A. Tyson, and C. Natoli, Solid State Communication **78**, 265 (1991).
[4] M. Newville *et al.*, Physica B: Condensed Matter **208-209**, 154 (1995), proceedings of the 8th International Conference on X-ray Absorption Fine Structure.
[5] A. Filipponi, A. Di Cicco, and C. R. Natoli, Phys. Rev. B **52**, 15122 (1995).
[6] A. Filipponi and A. Di Cicco, Phys. Rev. B **52**, 15135 (1995).
[7] A. Filipponi and A. Di Cicco, TASK Quart. **4**, 575 (2000).
[8] GNXAS. Extended suite of programs for advanced x-ray absorption data-analysis: methodology and practice, edited by A. Di Cicco (TASK publishing, Gdansk, Poland, 2009).
[9] A. Filipponi and A. Di Cicco, Phys. Rev. B **51**, 12322 (1995).
[10] A. Filipponi, Journal of Physics: Condensed Matter **13**, R23 (2001).
[11] A. Filipponi, J. Phys.: Condens. Matter **6**, 8415 (1994).
[12] A. Trapananti and A. Di Cicco, Phys. Rev. B **70**, 014101 (2004).
[13] E. A. Stern, P. Līviņš, and Z. Zhang, Phys. Rev. B **43**, 8850 (1991).
[14] A. Di Cicco and A. Filipponi, Europhys. Lett. **27**, 407 (1994).
[15] A. Witkowska, J. Rybicki, S. D. Panfilis, and A. Di Ciccoli, Journal of Non-Crystalline Solids **352**, 4351 (2006), proceedings of the 3rd International Conference on Physics of Disordered Systems (PDS 05).
[16] A. Di Cicco, M. Minicucci, and A. Filipponi, Phys. Rev. Lett. **78**, 460 (1997).
[17] A. Di Cicco, A. Trapananti, S. Faggioni, and A. Filipponi, PRL **91**, 135505 (2003).
[18] A. Di Cicco and A. Trapananti, J. Phys.: Condens. Matter **17**, S135 (2005).
[19] A. Di Cicco *et al.*, Applied Physics Letters **89**, 221912 (2006).
[20] A. Di Cicco and A. Trapananti, J. Non-Cryst. Sol. **353**, 3671 (2007), proceedings of the 12th International Conference on Liquid and Amorphous Metals.
[21] A. Di Cicco *et al.*, Phys. Rev. B **89**, 060102 (2014).
[22] O. J. Eder *et al.*, J. Phys. F: Metal Phys. **10**, 183 (1990).
[23] Y. Waseda, The Structure of Non-Crystalline Materials (McGraw-Hill, New York, 1980).
[24] A. Di Cicco and A. Filipponi, Journal of non-crystalline solids **156**, 102 (1993).
[25] L. Ottaviano *et al.*, J. Non-Cryst. Sol. **156-158**, 112 (1993).
[26] L. Ottaviano, A. Filipponi, and A. Di Cicco, Phys. Rev. B **49**, 11749 (1994).
[27] A. Di Cicco, Phys. Rev. B **53**, 6174 (1996).
[28] A. Filipponi *et al.*, Phys. Rev. E **48**, 4575 (1993).
[29] A. Filipponi, P. D' Angelo, N. V. Pavel, and A. Di Cicco, Chem. Phys. Lett. **225**, 150 (1994).
[30] A. Filipponi and A. Di Cicco, Nucl. Instr. Meth. B **93**, 302 (1994).
[31] A. Di Cicco and A. Filipponi, Journal of Non-Crystalline Solids **205–207**, 304 (1996).
[32] A. Di Cicco, Phys. Rev. Lett. **81**, 2942 (1998).
[33] A. Di Cicco, S. Fusari, and S. Stizza, Philosophical Magazine B **79**, 2113 (1999).
[34] A. Filipponi *et al.*, J. Phys.: Condens. Matter **10**, 235 (1998).
[35] A. Di Cicco *et al.*, J. Non-Cryst. Sol. **352**, 4155 (2006).
[36] A. Di Cicco *et al.*, Journal of Physics: Conference Series **190**, 012043 (2009).
[37] P. D' Angelo *et al.*, J. Chem. Phys. **100**, 985 (1994).
[38] V. Migliorati *et al.*, Inorganic Chemistry **52**, 1141 (2013).
[39] A. Di Cicco, Journal of Physics: Condensed Matter **8**, 9341 (1996).
[40] A. Di Cicco *et al.*, J. Phys.: Condens. Matter **8**, 10779 (1996).
[41] T. M. Hayes, J. B. Boyce, and J. L. Beeby, J. Phys. C: Solid State Phys. **11**, 2931 (1978).
[42] T. M. Hayes and J. B. Boyce, J. Phys. C: Solid State Phys. **13**, L731 (1980).
[43] M. Minicucci and A. Di Cicco, Phys. Rev. B **56**, 11456 (1997).
[44] A. Di Cicco, M. Taglienti, M. Minicucci, and A. Filipponi, Phys. Rev. B **62**, 12001 (2000).
[45] S. De Panfilis, A. Di Cicco, A. Filipponi, and M. Minicucci, International Journal of High Pressure Research **22**, 349 (2002).
[46] A. Trapananti, A. Di Cicco, and M. Minicucci, Phys. Rev. B **66**, 014202 (2002).
[47] A. Di Cicco, E. Principi, and A. Filipponi, Phys. Rev. B **65**, 212106 (2002).
[48] D. A. Allen and R. A. Howe, Journal of Physics: Condensed Matter **4**, 6029 (1992).
[49] A. Di Cicco and A. Filipponi, in X-Ray Absorption Spectroscopy of Semiconductors, Vol. 190 of Springer Series in Optical Sciences, edited by C. S. Schnohr and M. C. Ridgway (Springer Berlin Heidelberg, ADDRESS, 2015), pp. 187–200.
[50] E. Principi *et al.*, Phys. Rev. B **74**, 064101 (2006).
[51] C. Bressler, , and M. Chergui, Chemical Reviews **104**, 1781 (2004), pMID: 15080712.
[52] S. L. Johnson *et al.*, Phys. Rev. Lett. **94**, 057407 (2005).
[53] B. I. Cho *et al.*, Phys. Rev. Lett. **106**, 167601 (2011).
[54] E. Allaria *et al.*, New Journal of Physics **14**, 113009 (2012).
[55] Y. Obara *et al.*, Opt. Express **22**, 1105 (2014).
[56] E. Principi *et al.*, Structural Dynamics **3**, 023604 (2016).
[57] J. P. Itié *et al.*, Phys. Rev. Lett. **63**, 398 (1989).
[58] E. Principi *et al.*, Phys. Rev. B **69**, 201201 (2004).
[59] A. Di Cicco *et al.*, Phys. Rev. B **78**, 033309 (2008).
[60] F. Coppari *et al.*, Physical Review B **80**, 115213 (2009).
[61] F. Coppari *et al.*, Phys. Rev. B **85**, 045201 (2012).
[62] G. Mancini, M. Celino, F. Iesari, and A. D. Cicco, Journal of Physics: Condensed Matter **28**, 015401 (2015).
[63] L. Properzi *et al.*, Scientific Reports **5**, 10188 (2015).
[64] A. Grzechnik, T. Grande, and S. Stlen, Journal of Solid State Chemistry **141**, 248 (1998).
[65] P. S. Salmon and I. Petri, Journal of Physics: Condensed Matter **15**, S1509 (2003).
[66] I. Petri, P. S. Salmon, and H. E. Fischer, Phys. Rev. Lett. **84**, 2413 (2000).
[67] W. Zhou, M. Paesler, and D. E. Sayers, Phys. Rev. B **43**, 2315 (1991).
[68] M. Durandurdu and D. A. Drabold, Phys. Rev. B **65**, 104208 (2002).
[69] Q. Mei *et al.*, Physical Review B **74**, 014203 (2006).
[70] M. Vaccari *et al.*, Phys. Rev. B **81**, 014205 (2010).